Lopez-Jauregi, A., Ulacia, I., Esnaola, J.A. et al. Procedure to predict residual stress pattern in spray transfer multipass welding. Int J Adv Manuf Technol 76, 2117–2129 (2015). https://doi.org/10.1007/s00170-014-6424-0

Procedure to predict residual stress pattern in spray transfer multipass welding

A. Lopez[a*], I. Ulacia[a], J.A. Esnaola[a], D. Ugarte [a], I. Torca[a]

[a] Mechanical and Manufacturing Department, Faculty of Engineering, Mondragon Unibertsitatea, Loramendi 4, 20500, Mondragon, Spain

[*]Corresponding author. Tel.: +34 943 73 96 67; Fax: +34 943 79 15 36

E-mail address: alopezj@mondragon.edu (A. Lopez)

Abstract

Gas metal arc welding (GMAW) is one of the most used joining method in the industry. However, one of the main problems of this process is the generation of residual stresses which have direct impact on the fatigue life of welded components. Nevertheless, residual stress pattern prediction is complex and requires the simulation of the welding process. Currently, there are different numerical methods to predict the residual stresses generated in GMAW process, being Goldak's method one of the most widely used model. However, the main limitation of these methods is that they require defining many parameters experimentally and consequently this method is not valid during design process.

Alternatively, in this work, it is developed a procedure where the heat source is defined based on the welding physics for spray transfer welding. The developed procedure has been validated for a spray transfer multipass butt weld case. Results have shown good correspondence with an average deviation of 9.16% in thermal field and 42 MPa in the final residual stress field. Thus, the developed procedure has been validated as a cost effective alternative method to estimate residual stress pattern in spray transfer multipass welding. Furthermore, the developed method does not require any welding experimental characterization once the efficiency of the used welding machine is defined. The proposed method can be used as a valid tool to optimize the welding process in order to minimize the residual stress field and, consequently, improve the fatigue life.

Keyword: Multipass Welding, Analytic procedure, Finite element method, Equivalent heat source, Temperature distribution, Residual stresses.

1 Introduction

Welding process is nowadays, the third method employed in the metal manufacturing industry [1]. Among the different welding techniques, the gas metal arc welding (GMAW), also referred as a metal inert gas (MIG), is one of the most widely used due to its high productivity [1], [2]. Particularly, spray transfer mode multipass welding is especially suitable when joining high thickness structures [3, 4] due to the high rate of metal transfer, high arc stability, absence of weld spatter, and uniform and regular metal transfer to the workpiece.

However, one of the main problems of welded structures is the generation of residual stresses which have a direct impact on the high cycle fatigue life behaviour [5, 6]. Residual stresses are generated due to high thermal cycles in the welding process where non-uniform heating and cooling occur, generating inhomogeneous plastic deformation [5, 7]. In general, tensile residual stresses are considered detrimental because they increase the susceptibility of the welded joint to fatigue damage, stress-cracking-corrosion (SCC), structural buckling and brittle fracture [7, 8, 9].

The estimation of residual stress pattern in welded structures is very complex since many complicated physical phenomena as heat, electricity, or mechanical work take part in them [10, 11]. Furthermore, the distribution of welding residual stresses depends on several factors such as structural dimensions, welding sequence, preparation of the weld groove, mechanic restraints or the number of weld pass [12, 13, 14]. Therefore, in order to make a less conservative design of welded components it is necessary to consider the magnitude and distribution of residual stresses [7, 11, 15]. The accurate measurement of residual stresses nowadays present some limitation as

experimental methods still are not fully reliable [14, 15, 16]. In addition, it implies huge time and economic cost. Due to the practical difficulties that arise in measuring residual stresses within thick components, these stresses are obtained by combining experimental measurements with predictions from numerical models [9].

One of the most critical aspects when simulating welding processes is the moving heat source modelling [19]. The first research on the heat source modelling was made in the early 1940s, where Rosenthal proposed an analytical model for the moving heat source [20]. This model assumes quasi or pseudo steady state (after a certain time from the weld is started) and a concentrated point heating. This method is only valid for simple geometries and it has a lack of precision for plates with certain thickness [2, 7]. In the late 1960s, Pavelic et al. [21] proposed to model the heat source like a circular disc with Gaussian distribution on the surface of the workpiece. This model does not take into account the heat transfer through the fusion zone and it is not possible to predict the depth of penetration.

Nowadays, one of the most widely used method to model the heat source during the GMAW process is the Goldak's method [22, 23, 24, 25, 26, 27]. In this model, the heat source is approximated as a double ellipsoidal power density distribution. The main limitation of this method is that it requires measuring the weld pool, which should be done during or after finishing the welding process. For this reason, its application as a predictive method is limited [28]. Also in certain welded joints, T-joints, L-joints… the weld pool measurement for each pass is geometrically limited and sometimes cannot be conducted. Wahab et al. [29] developed some analytical equations, based on experimental measurements, to define the geometry of the weld pool depending on the

voltage, the current, the welding speed and the percentage of carbon dioxide (% CO2). However, this alternative shows still limitation with a maximum deviation higher than 100 MPa in the residual stress estimation [8].

Brickstad et al. [12] developed another technique in which as input parameters they used the current and the voltage applied in the welding process. They employed a two-dimensional axisymmetric model to numerically simulate multi pass butt-welds of stainless steel pipes. However, their model was not validated against experimental tests. Barsoum et al. [30], also used the same technique in a three dimensional model to simulate a multi-pass welding of tubular joint and this model was validated by experimental tests. In the case of thermal field validation, the method developed by them presented good accuracy for the specific case of a single pass butt weld. However, in the two pass butt welded plate, the thermal field results show lower accuracy. Regarding to the residual stress field, in both cases the longitudinal residual stresses are in good agreement with the experimental results but in the case of transverse residual stresses in butt welds shows a poor agreement with experimental measurements. The heat source was modelled using the tuning approach, which in case that experimental data is available, consist in setting the calculated temperature histories into agreement with those experimental data measured by the thermocouples. In the case that there is no experimental data available, the welding parameters are adjusted to achieve a reasonable molten zone size and distance to the HAZ from the fusion zone boundary [31].

Finally, some authors have used a 3D mathematical model for the plasma arc and metal transfer in order to solve accuracy limitations [32, 33, 34]. This method, besides the computational cost, requires defining properly several parameters such as arc plasma

viscosity, arc plasma temperature, surface tension coefficient, etc. The complexity for determining those parameters together with high computational cost limits the use of this technique.

As an alternative, in the present work an analytic procedure to calculate the welding process key parameters is presented which will feed FEM numerical model. This procedure is based on the welding physics for spray transfer and the main advantage is that it does not require any experimental values a priori. To verify the developed procedure, the heat source model has been experimentally verified first and then, the implemented FEM model results have been compared against thermal pattern history and final residual stress pattern measurements. The main contribution of the presented procedure is that it provides an agreement between the accuracy of the model in the residual stress estimation, the computational cost and the model definition effort. Besides, the new procedure does not require any preliminary experimental welding tests data and the used model parameters are easy to obtain by defining the standard parameters of the welding process.

2 Modelling procedure

One of the critical aspects in order to feed the FEM spray transfer multipass welding as a predictive tool is the determination of the process input parameters, heat source and welding speed. For that purpose, an analytic procedure to determine the heat source and welding speed, ensuring proper spray transfer welding, is developed.

Thus, the proposed process modelling procedure consists of two steps. First, the process key parameters are defined based on the developed analytic procedure. Then, the

definition of the FEM uncoupled thermo-mechanical model is described. This numerical model is fed from the previously defined parameters.

2.1 *Heat source and welding speed determination*

The necessary input parameters to feed the multipass spray transfer welding FEM model are the heat source energy and the welding speed. Those two parameters are defined based on the welding conditions for spray transfer, in accordance with the cross section to weld and the welding torch configuration. Fig. 1 shows the detail of the configuration of the welding torch, where L_{arc} is the arc length, L_{CTW} is the contact to work distance and L_{so} is the wire extension or electrical stick-out length.

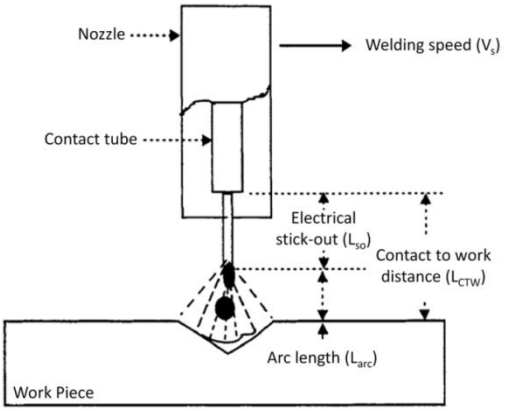

Fig. 1 Configuration of the welding torch (adapted from [1]).

- *Heat source energy:*

The heat source energy is the total thermal energy which is provided to the weld bead along the process. This parameter is obtained taking into account the process efficiency, i.e. the heat power transformation from the total consumed electric power. Thus, the heat power supplied for spray transfer could be obtained with the equation (1):

$$P_{\mathrm{TH}} = \eta \cdot I \cdot V_{\mathrm{Tot}} \quad (1)$$

where P_{TH} is the supplied thermal power, η is the heat transformation efficiency, I is the current intensity and V_{Tot} is the total voltage.

As it is widely known, energy losses occur due to the wire resistance, losses to the surroundings, gas or flux heating, etc. According to the literature, the efficiency η can vary between 0.66 and 0.85 [1].

In order to determine the welding intensity I, the transition welding intensity between globular transfer and spray transfer is determined first. This parameter depends on the used shielding gas and the welding wire diameter. Thus, based on the correlation proposed by Norrish (Fig. 2) [30], the transition welding intensity between globular transfer and spray transfer mode is determined. Consequently, in order to ensure spray transfer welding condition the applied welding intensity has to be higher than the limit value.

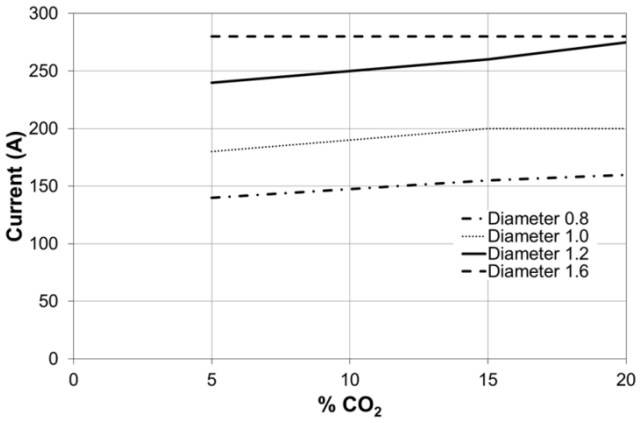

Fig. 2 Relationship between the composition of the shielding gas and the transition current, for carbon steel wires diameter range between 0.8 and 1.6 mm [35].

The total voltage drop V_{Tot} is approximately the addition of the voltage drop in the electric stick-out length V_{so} and the voltage drop across the arc V_{arc} (2) [1]:

$$V_{\mathrm{Tot}} = V_{\mathrm{arc}} + V_{\mathrm{so}} \tag{2}$$

The arc voltage drop can be obtained with equation (3):

$$V_{\mathrm{arc}} = I \cdot R_{\mathrm{arc}} + a_0 + a_1 \cdot L_{\mathrm{arc}} \tag{3}$$

where R_{arc} is the arc electric resistance, a_0 is the anode/cathode voltage drop and a_1 is the arc potential gradient. The minimum L_{arc} to ensure spray transfer has to be higher than 4.5mm according to Lesnewich [36].

The voltage drop across the electrode is calculated with the equation (4):

$$V_{\mathrm{so}} = \rho_{\mathrm{s}} \frac{L_{\mathrm{so}}}{A_{\mathrm{so}}} I \tag{4}$$

where ρ_{s} is the resistivity of the stick-out material and A_{so} is the cross section area of the wire.

The stick-out length L_{so} (Fig. 1) is determined with the equation (5):

$$L_{\mathrm{so}} = L_{\mathrm{CTW}} - L_{\mathrm{arc}} \tag{5}$$

- *Welding speed:*

The welding speed is the velocity the welding torch advances along the welding bead. It is assumed that GMAW process fulfils the mass conservation law. Thus, wire feed speed and welding speed can be correlated by the following equation (6):

$$A_{\mathrm{so}} \cdot v_{\mathrm{w}} = A_{\mathrm{s}} \cdot v_{\mathrm{s}} \;\rightarrow\; v_{\mathrm{s}} = \frac{A_{\mathrm{so}} \cdot v_{\mathrm{w}}}{A_{\mathrm{s}}} \tag{6}$$

where v_{w} is the wire feed speed, A_s is the weld pass cross section and v_{s} is the welding speed.

There are two approaches to model the wire feed rate for constant voltage welding used in GMAW as suggested by Palani et al. 2007 [37]: the first approach is to conduct welding experiments to fit the equation relating welding current and wire feed

rate; the second one is to use the results of the experiments to determine the constants of proportionality for arc heating and electrical resistance heating.

In the present work, the second approach is used, where the relationship between wire feed speed and current is given by the parabolic model of equation (7) [35]. In literature different works that determine the constants of proportionality for arc heating and electrical resistance heating regarding wire cross section are available, i.e. solid or cored wire. In the present study solid wire is used and therefore values obtained for cored wire cannot be used.

$$v_{\mathrm{w}} = \alpha \cdot I + \frac{\beta \cdot L_{\mathrm{so}} \cdot I^2}{A_{\mathrm{so}}} \tag{7}$$

where α and β are constants dependent on the used wire properties.

Moreover, considering different values of the constants (α and β) from several studies for solid plain carbon steel wire analysed from literature ([35], Murray 2002, Modenesi 2007, Palani 2006, Palani 2007) it is observed that their difference is negligible. Therefore, in the present work it is decided to consider the values defined in [35], α ≈ 0.3 mmA-1s-1 and β ≈ $5 \cdot 10^{-5}$ A-2s-1 for a 1.2 mm plain carbon steel wire.

2.2 *Multipass welding FEM modelling procedure*

- *Geometric model:*

The case study of the present work (Fig. 3 a)) is a 3 pass spray transfer butt weld of 10 mm thick, 200 mm length of two S275JR steel plates. Based on the calculated cross section, the critical geometric feature to define the weld bead is the definition of bead radius. Teng et al. [41], observed that the influence of the flank angle in the residual stress value has been observed negligible. Thus, based on real geometry of welded plates, a 30º flank angle has been selected to define the bead radius. Then the

arc of the last pass bead can be defined by constraining the tangency with the auxiliary curves at 30º flank angle (see Fig. 3) and the two points of the edge of the weld toe for the last pass. The arcs for the bead in the rest of the passes are defined concentric with respect to the last pass by keeping the value of the initially calculated cross section for each pass.

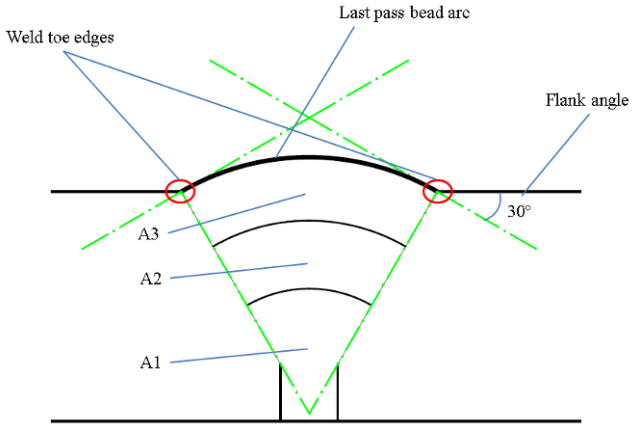

Fig. 3 Procedure to calculate the weld bead geometry for each pass.

The model is meshed by using full integration continuum hexahedral elements and the addition of filler material through the tree passes has been modelled by using the kill/rebirth method [13, 19, 23] (Fig. 4 b) and Fig. 4 c)). In this method all the weld bead elements are initially inactive and, consequently, eliminated from the equation system. Elements are activated in function of the welding speed (v_s), simulating the welding torch pass.

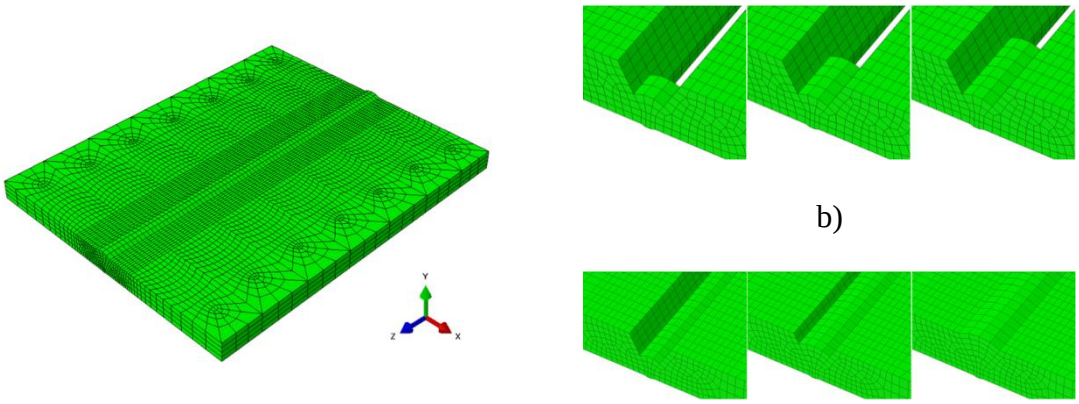

Fig. 4 a) Model used for the simulation of the welding process, b) Principle of the addition of the weld bead and c) Multipass welding modelling.

In order to determine the activation length of the weld bead, a preliminary sensitive analysis has been performed. It has been observed that discretisation levels up to 20 mm length provide quite stable temperature results. However, in order to validate the transient temperature evolution a temporal discretization of one second has been specified. Thus, the critical activation length per second of 6.12 mm is identified for the third pass, which is conducted with the lower welding speed for the same wire speed. Consequently, a 5 mm length discretization size, which ensures a temporal discretization < 1s for the three passes, is selected for the presented work. Furthermore, allows fitting exactly with 40 discretization volumes the 200 mm length of each pass.

- *Computational technique:*

The selected formulation to solve the mechanical and thermal fields along the welding process is an uncoupled thermo-mechanical method implemented in the simulation software ABAQUS^{TM}. The uncoupled approach is considered suitable as dimensional changes in the welding process can be accepted as negligible and mechanical deformation energy is insignificant compared to the thermal energy from

the welding arc [8]. Both equation systems, thermal and mechanical, are solved by using the implicit direct integration method.

- *Material:*

The welded plate material is S275JR and the filler material is PRAXAIR M-86 according to the AWS/ASME SFA 5.18 ER70S-6 standard. Table 1 shows the standard mechanical properties of both materials at room temperature. As it can be observed, both materials show similar ultimate strain and ultimate strength, but the yield stress of the filler material is 45% higher.

Table 1 Standard mechanical properties of S275JR structural steel [42] and PRAXAIR M-86 filler material, [43, 44].

	σ_y (MPa)	σ_u (MPa)	A (%)	E (GPa)
S275JR	275	430-580	23	190-210
Filler M-86	>400	>480	>22	200

Due to limitations obtaining the thermomechanical properties of the filler material, a temperature dependent yield stress 45% higher than the base material has been considered. The remaining materials thermo-mechanical properties for the filler material are assumed to be the same as the base material. This simplification has been considered acceptable based on the following assumptions:

- Thermal properties as conductivity, specific heat, latent heat or thermal expansion of both steels are similar. Consequently, assuming base material's thermal properties for the filler material will have minor influence in the computed temperature pattern and thermal expansion. These two parameters have direct influence in the predicted residual stress pattern.

- Minor variations in alloy content in structural steels have negligible influence on temperature dependent density or young modulus [45]. Thus, these two parameters can be considered similar for both materials.
- Yield stress of filler material is assumed to be 45% higher than the plate material at different temperatures, as at room temperature. Considering the low plastification level during the welded process same plastic tangent modulus can be considered when estimating filler material's temperature dependant stress/strain curves.
- The weld seam material cross section is small compared to both plates cross section. Therefore, the thermal expansion deviation in the weld seam section can be considered insignificant with respect to the total cross section thermal expansion. Consequently, the influence of the possible error generated from the previous assumptions in the computed residual stress in the perpendicular direction, which mainly affects the crack growth in welded plates' fatigue, will be negligible.

Thermal properties

Fig. 5 a), shows the utilized temperature dependent density, thermal conductivity and specific heat data for both, filler and plate materials. Table 2 shows the considered latent heat and solidus-liquidus transition temperature.

Table 2 Latent heat of fusion [34].

Latent heat (kJ/kg))	Solidus temperature (ºC)	Liquidus temperature (ºC)
247	1500	1550

Thermo-mechanical properties

Fig. 5 b), c) and d) shows the temperature dependent mechanical properties for both, the base material and filler material.

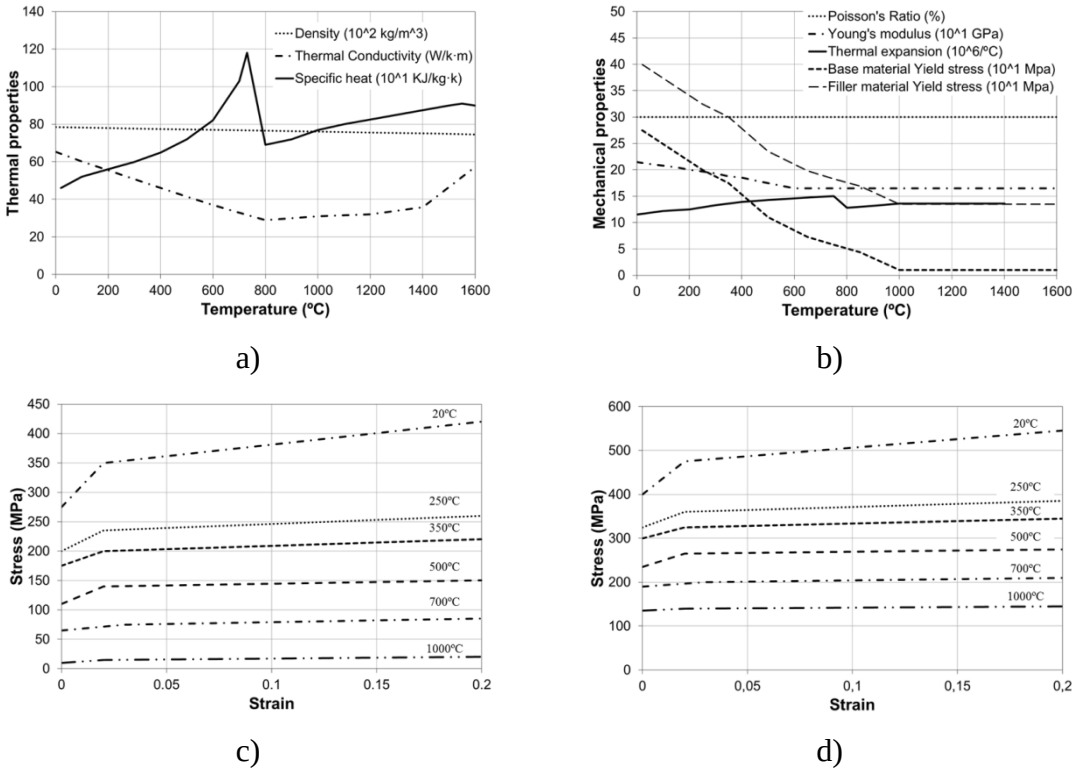

Fig. 5 Temperature dependant material properties. a) Specific heat is taken from [46], thermal conductivity is taken from [19, 47] and density is taken from [48], b) Young's modulus and thermal expansion are taken from [49] and yield stress is taken from [50, 51], c) plastic properties for the base material [19] and d) estimated plastic properties for the wire material.

In this work the phase transformation effect it is neglected since for the low carbon steels it has an insignificant effect in residual stresses and distortions. This is due to the small dilation that material suffers by martensitic transformation and a relatively high transformation temperature range [48].

- *Loads and boundary conditions:*

Heat transfer simulation

Based on the previously explained analytical procedure heat source and welding speed are defined for the specific case study of the present work.

Heat source power to be implemented as a uniform body heat flux in each activation volume has been calculated for each pass (Table 3) based on the following parameters:

- Efficiency: Simulations for an efficiency range between 0.6 and 1 have been performed in order to specify the efficiency of the used welding facility by comparing numerical temperature patterns and experimentally measured pattern.
- Welding Intensity: A transition welding intensity of 245 A has been determined for the used 1.2 mm wire diameter and shielding gas Stargon 82 (8% CO_2 [52]). Then, a welding intensity of 275 A, 12% over the transition limit, has been selected.
- Wire properties: For the used wire R_{arc} is 0.0237 Ω [3] and the values of a_0 and a_1 are 6.3 V and 1.55 V/mm respectively [4].
- Welding torch configuration: an arc length L_{arc} of 9 mm (> $L_{\mathrm{arc\_min}}$ of 4.5mm [36]) and L_{CTW} of 30 mm are defined. A resistivity ρ_{s} of the stick-out material of 0.2821 $\frac{\Omega}{m}$, for carbon steels [1], has been used.

Table 3 Values of the heat power for different efficiencies.

Efficiency (%)	Power (W)		
	First pass	Second pass	Third pass
1	7755	7755	7755
0.9	6980	6980	6980

0.85	6592	6592	6592
0.8	6204	6204	6204
0.75	5816	5816	5816
0.7	5429	5429	5429
0.6	4653	4653	4653

Welding speed to be implemented as element rebirth rate has been calculated for each pass by using the parabolic model constants $\alpha \approx 0.3$ mmA-1s-1 and $\beta \approx 5 \cdot 10^{-5}$ A-2s-1 for a 1.2 mm plain carbon steel wire [35]. Thus, the calculated welding speeds for each pass of the case study in the present work are 550, 480 and 370 mm/min.

Finally, a natural convection boundary condition has been assumed in all surfaces exposed to air of both plates and the rebirthed weld bead elements

Uncoupled thermo-mechanical simulation

Temperature pattern at every iteration is feed from the previously run heat transfer simulation results. As a boundary condition, one of the plate end surfaces has been assumed to be encastred.

3 Experimental procedure

A CNC milling machine and a welding machine Praxair Phoenix 421 have been adapted to perform the welding process automatically (Fig. 6). This way, all process parameters such as welding speed, arc length, contact to workpiece length, voltage and wire feed speed are controlled during the whole process ensuring stable data. In order to validate the proposed modelling procedure, temperature pattern evolution during the welding process and residual stresses of the welded samples are measured.

In addition, current intensity and voltage are monitored during the welding process with a TPS2024B Tektronix oscilloscope, a LEM PR 200 ammeter and a PR

HAMEG HZ115 voltmeter in order to verify the consumed instantaneous and total electric power.

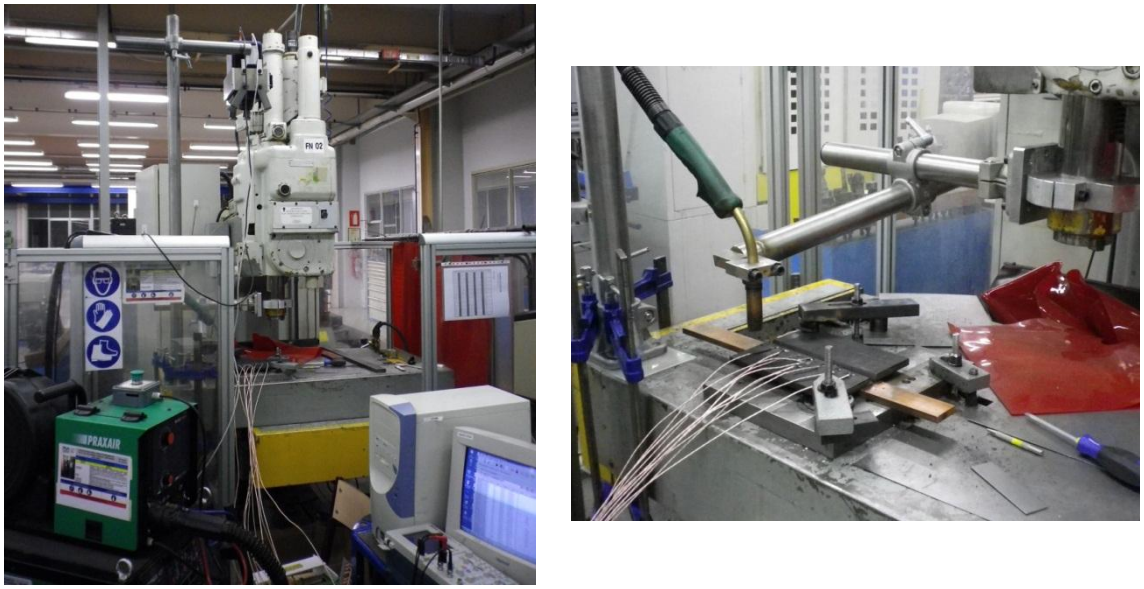

a) b)

Fig. 6 Set-up developed to perform automatically the welding process.

3.1 *Welding procedure*

10 mm thick 200 mm length S275JR plates are butt welded in three passes (Fig. 7) with 1.2mm diameter PRAXAIR M-86 filler material. Stargon 82, with 8% of CO2 [52], is used as shielding gas.

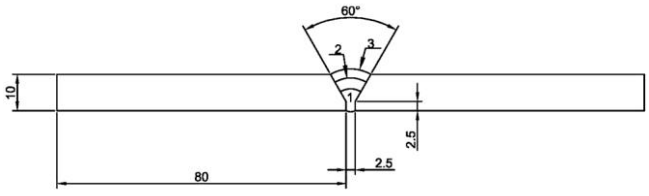

Fig. 7 Geometry of the plates and the weld bead for the butt joint model.

Welding process parameters for each pass are previously determined with the proposed analytical procedure for spray transfer mode (Table 4).

Table 4 Welding process parameters.

Pass	V (V)	I (A)	Vw (m/min)	P (W)	Larc (mm)	Lctw (mm)	Vs (mm/min)
1	28.2	275	9.2	7755	9	30	545.33
2	28.2	275	9.2	7755	9	30	482.83
3	28.2	275	9.2	7755	9	30	367.796

3.2 *Temperature pattern measurement*

Temperature pattern during the welding process is measured with a double objective: to determine welding facility's efficiency and to validate the numerically obtained temperature pattern evolution.

With this purpose temperature history along the whole process is acquired in parallel by both methods: thermocouples and thermographic camera. For that purpose, 10 N-type thermocouples (up to 1200ºC) are placed parallel and perpendicular to the weld bead as shown in Fig. 8 a) and a Titanium DC019U-E thermographic camera is used to record surface temperature pattern. Plates are painted with a high temperature resistant black colour paint which temperature dependent emissivity is already determined [53]. However, for better accuracy, acquired temperature pattern is calibrated with thermocouples acquisition data.

3.3 *Residual stress measurement*

Residual stresses of welded samples are measured by hole-drilling method in order to validate numerically obtained residual stress pattern and, consequently, to validate the procedure proposed in the present work.

To conduct the measurements, Vishay EA-06-062RE-120 rosette type gauges are placed parallel to the welding bead, at a 52.5 mm distance from the weld toe at both

sides of the weld bead as shown in Fig. 8 b). Then, hole-drilling tests are carried out in a CNC milling machine according to ASTM E837 standard.

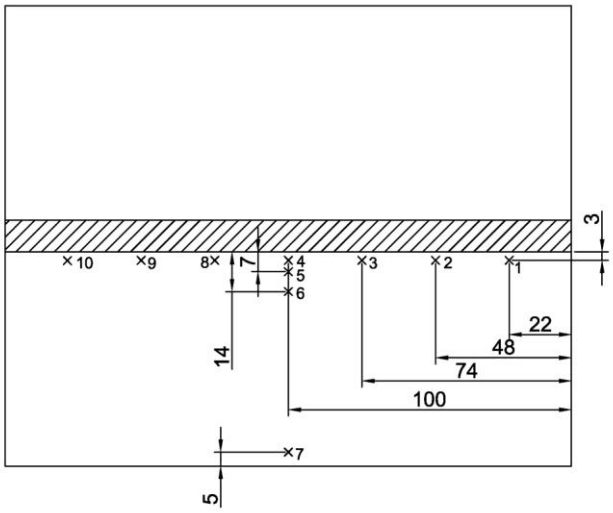

a)

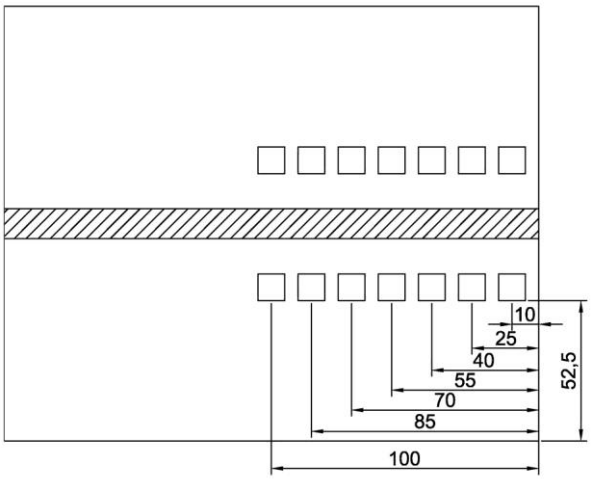

b)

Fig. 8 a) Position of the thermocouples and b) Position of the hole-drilling gauges in the butt weld.

4 Results and discussion

In this section, the developed modelling procedure is validated against experimental results. Validation is carried out in two steps. First, the temperature pattern prediction is validated, as it is directly related with material's thermal expansion. Then residual stress pattern caused by thermal expansion is validated.

4.1 *Temperature pattern validation*

Temperature pattern for the ideal case with an efficiency value of 1 is compared first against experimental measurements (Fig. 9). It is observed that the proposed model shows similar process dynamics: a high temperature increase occurs when the welding torch is near to the thermocouple took as reference, followed by a progressive cooling down due to heat evacuation. Heat is mainly evacuated through conduction to the plates and convection to the air. It is observed that peak temperature for each pass increases as the provided heat is higher than the evacuated heat from pass to pass. However, as expected, the estimated quantitative temperature values are higher than the experimentally obtained as no power losses are considered (Fig. 9).

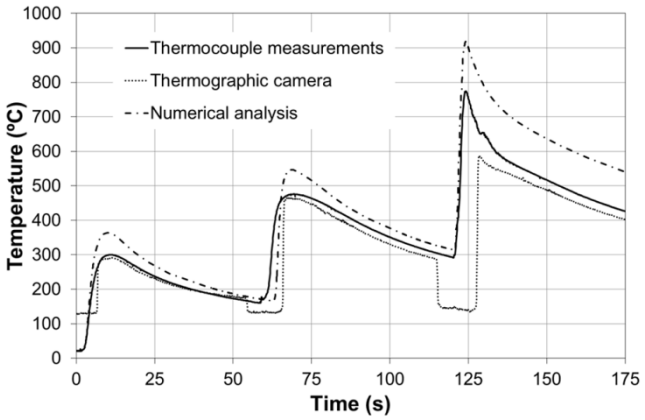

Fig. 9 Calculated and measured thermal cycles for the first thermocouple with an efficiency factor of 1.

In order to determine the efficiency of the system, peak temperature deviation in each pass and for all thermocouples (transversal and longitudinal direction) with different efficiency values, between 0.6-1, is compared against experimental results (Table 5). It is observed that an efficiency value of 0.8 provides the best accuracy along the three passes with an average deviation of 9.16%. Therefore, an efficiency value of 0.8, which is in accordance with other authors estimation (0.66-0.85) [1], is established for the used welding facility.

Table 5 Calculated error for the peak temperatures at each pass for an efficiency range of 0.6-1.

Efficiency	Error (%)			
	First pass	Second pass	Third pass	Average
1	21.9	20.0	21.8	21.2
0.9	12.8	10.5	16.7	13.3
0.85	8.5	5.8	16.7	10.3
0.8	3.9	5.3	18.3	9.2
0.75	3.5	6.6	19.8	9.9
0.7	6.6	9.9	21.4	12.7
0.6	17.4	20.2	31.2	22.9

Fig. 10 shows the comparison of temperature evolution at thermocouple 1 location among the predicted for efficiency of 0.8 and the experimentally measured. A thermocouple positioning error of +/-0.5 mm has been considered in the temperature validation. As it is observed, temperature evolution shows positive correspondence along the three passes.

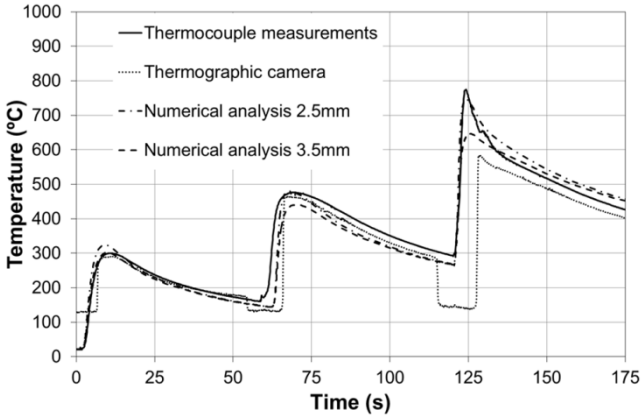

Fig. 10 Comparative of experimental versus FEM thermal results for a butt weld with an efficiency factor of 0.8.

In addition, Fig. 11 shows the comparison between the experimental temperature pattern acquired with the thermographic camera and the numerically predicted pattern for an efficiency value of 0.8 at the end of each pass. It can be observed that both temperature pattern show positive correspondence along the three passes with similar isothermal contours. Thus, at each pass the high temperature zone, over 700ºC show similar shape and length as well the cooling down temperature contours down to 300ºC (limit of the used thermographic camera's filter).

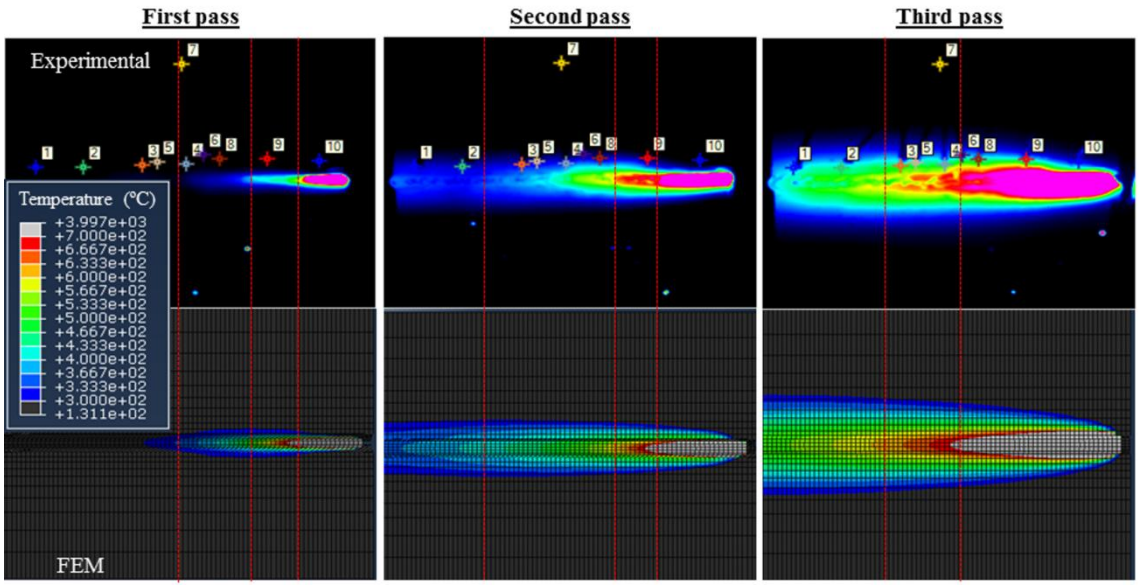

Fig. 11 Comparative of experimental versus FEM thermal pattern for a butt weld with an efficiency factor of 0.8. (The points in the upper images are the position of the thermocouples).

Considering the low deviation (9.16%) in the temperature evolution prediction through the three passes as well as the good correspondence of the temperature pattern contours at each pass, the numerical procedure to predict temperature pattern evolution of multipass spray transfer welding is validated.

4.2 *Residual stress validation*

In order to end up the validation of the proposed numerical model the residual stress field is verified.

Fig. 12 shows transverse residual stresses pattern obtained through FEM uncoupled thermo-mechanical simulation. High stress concentration is estimated in the restricted area where 6 degrees of freedom are fixed (in accordance with the experimental setup). However, these stress concentration areas are located far enough

from the area of interest and they are not considered in the residual stress validation process. Focusing in the area of interest, a mild asymmetry is observed between the weld toes at both sides of the weld seam as asymmetric mechanical restrictions are applied. Thus, in order to validate the predicted residual stresses, path 1 and path 2 are defined in the maximum stress area, parallel to the weld seam as shown in Fig. 12. Then the residual stresses along both paths are compared against experimental measurements.

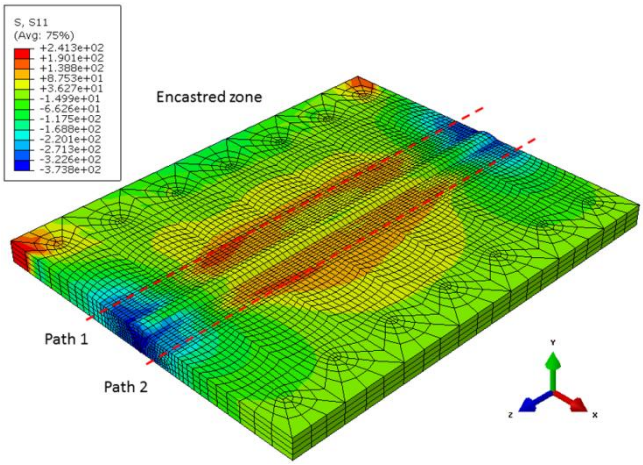

Fig. 12 Transversal residual stresses pattern for a butt weld.

Fig. 13 shows transversal residual stress hole-drilling measurements along half of the length (0-100 mm) for both, path 1 and path 2. It can be distinguished three zones: compression zone (0-30 mm), transition zone (30-60 mm) and tensile zone (60-100 mm). As it can be observed, some measurements are made in the full length (at 160mm and 175mm) in order to verify that the residual stresses along the weld seam direction are quasi-symmetric.

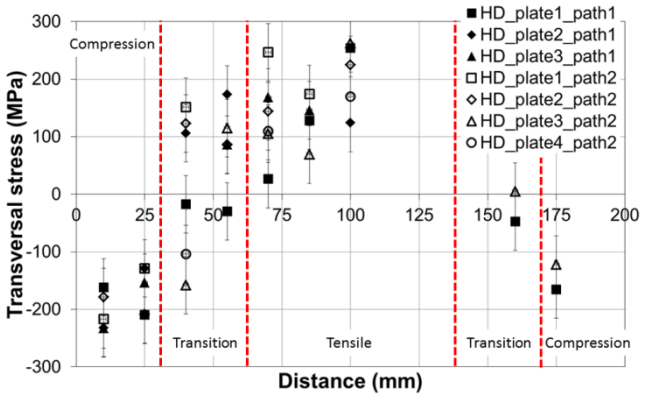

Fig. 13 Results of Hole-drilling measurements for different plates and for both paths.

High scatter among the several measurements carried out at each measuring position is observed, inherent of the measuring technique. According to some authors, up to ± 50 MPa measurement deviations have been reported for this technique [17].

Thus, in order to perform the residual stress validation, the average hole-drilling result at each position for both paths is obtained. Fig. 14 a) and Fig. 14 b) show the comparison between the average hole-drilling results with their standard deviation and simulation results for path 1 and path 2 respectively. It can be observed a positive correspondence between the averaged measurements and the numerical results for both paths. Thus, compression zone, transition zone and tensile zone show similar trends. Regarding to both paths, an average error of 34 MPa, 35 MPa and 57 MPa for each zone respectively is calculated with an average total error of 42 MPa. As observed, numerically predicted residual stress values are mostly inside the measurement scatter band (±50 MPa [17]).

It must be noted that the numerical model does not predict the residual stress peak observed at the middle of the plate (100 mm) in the experimental results. Due to this,

maximum deviation is observed in the tensile zone where simulation estimates a quasi-uniform value of residual stresses. The reason for this stress peak can be that the boundary conditions in the numerical model are not properly defined. Regarding to the transition zone, simulation estimates slightly softer transition than the experimental results.

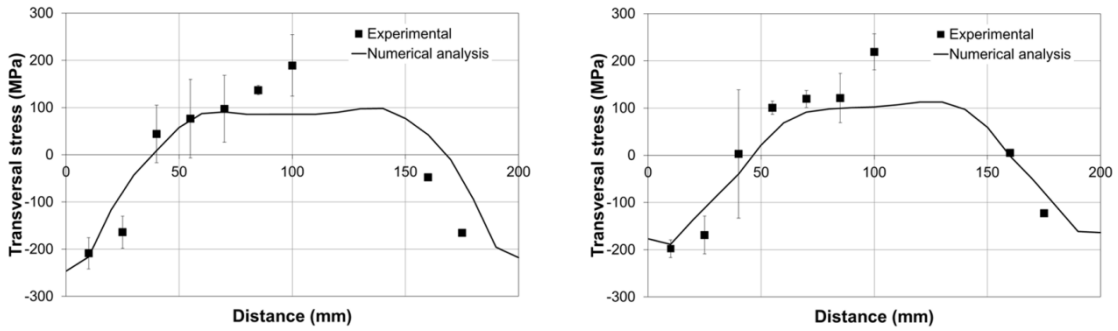

a) b)

Fig. 14 Comparison of the FEM and experimental results for the Results of Hole.

In summary, numerically obtained residual stress curves show similar trends with residual stress magnitude inside the measuring technique scatter band (±50 MPa [17]). Thus, taking into account the actual measuring technique limitation numerical results can be considered valid with an average error of 42 MPa.

5 Conclusions

In this study, in order to predict temperature evolution and residual stress pattern in multipass spray transfer welding, an analytic procedure to calculate the welding process key parameters is proposed and validated. The proposed procedure could be extended to other gas metal arc welding processes. In addition, this procedure enables to perform welding process simulation without any experimental test to define input parameters for the numerical model, once the welding machine's efficiency is

determined. For general purpose, efficiency values between 0.66-0.85 according to other authors can be used [1].

Based on the results obtained in this study, it is proved that the suggested model overcomes the need of experimental data. Thus the procedure reaches to a compromise between the precision in the temperature pattern (9.16% average error) and residual stresses (42 MPa average error) prediction and the simplicity defining the model input parameters as well as the required computational cost. Therefore, authors consider that the proposed procedure is a very effective tool to model multipass spray transfer welding. The suggested modelling method can be used to optimize the welding process in order to minimize the residual stress field and, consequently, improve the fatigue life.

Aknowledgment

The authors wish to express their gratitude for the financial support by the ministry of science and innovation through the national program of public-private cooperation INNPACTO 2011. Iñaki Martinez, Hector Olarte and Aritz Frojan (from Fagor Arrasate S. Coop) and Aitor Garro (from Koniker S. Coop) are also acknowledged for their helpful comments and discussions.

References

1. Naidu DS, Moore KL, Ozcelik S (2003) Modeling, sensing and control of gas metal arc welding. Kidlington (UK): Elsevier Science Ltd
2. Gery D, Long H, Maropoulos P (2005) Effects of welding speed, energy input and heat source distribution on temperature variations in butt joint welding. J Mater Process Technol 167(2): 393–401

3. Mousavi M, Haeri M (2011) Estimation and control of droplet size and frequency in projected spray mode of a gas metal arc welding (GMAW) process. ISA T 50(3): 409–418
4. Murray PE (2002) Selecting parameters for GMAW using dimensional analysis. Weld J 81(7): 125–131
5. Maddox SJ (1991) Fatigue strength of welded structures. Woodhead publishing
6. Kong F, Ma J, Kovacevic R (2011) Numerical and experimental study of thermally induced residual stress in the hybrid laser-GMA welding process. J Mater Process Technol 211(6): 1102-1111
7. Sattari-Far I, Farahani MR (2009) Effect of the weld groove shape and pass number on residual stresses in butt-welded pipes. Int J Pres Ves Pip 86(11): 723–731
8. Deng D, Murakawa H (2006) Numerical simulation of temperature field and residual stress in multi-pass welds in stainless steel pipe and comparison with experimental measurements. Comp Mater Sci 37(3): 269–277
9. Turski M, Francis JA, Hurrell PR, Bate SK, Hiller S, Withers PJ (2012) Effects of stop-start features on residual stresses in a multipass austenitic stainless steel weld. Int J Pres Ves Pip 89: 9–18
10. Messler RW (2008) Principles of welding. John Wiley & Sons
11. Chang PH, Teng TL (2004) Numerical and experimental investigations on the residual stresses of the butt-welded joints. Comp Mater Sci 29(4): 511–522
12. Brickstad B, Josefson BL (1998) A parametric study of residual stresses in multi-pass butt-welded stainless steel pipes. Int J Pres Ves Pip 75(1): 11–25

13. Keivani R, Jahazi M, Pham T, Khodabandeh AR, Afshar MR (2014) Prediction residual stresses and distortion during multisequnce welding of large size structures using FEM. Int J Adv Manuf Technol 1-11
14. Asadi M, Goldak J, Nielsen J, Zhou J, Tchernov S, Downey D (2009) Analysis of predicted residual stress in a weld and comparison with experimental data using regression model. Int J Mech Mater Des 5: 353-364
15. Paradowska A, Price J, Ibrahim R, Finlayson T (2005) A neutron diffraction study of residual stress due to welding. J Mater Process Technol 164: 1099-1105
16. García V (2006) Optimización de procesos de mecanizado mediante control de tensiones residuales y otros parámetros de integridad superficial. PhD thesis, Campus tecnológico de la universidad de navarra
17. Withers PJ, Bhadeshia HKDH (2001) Residual stress. Part 1-measurement techniques. Mater Sci Technol 17(4): 355–365
18. Price J, Paradowska A, Joshi S, Finlayson T, Semetay C, Nied H (2008) Comparison of experimental and theoretical residual stresses in welds: The issue of gauge volume. Int J Mech Sci 50: 513-521
19. Hansen JL (2003) Numerical modelling of welding induced stresses. PhD thesis, Technical University of Denmark
20. Rosenthal D (1941) Mathematical theory of heat distribution during welding and cutting. Weld J 20(5): 220–234
21. Pavelic V, Tanbakuchi R, Uyehara OA, Myers PS (1969) Experimental and computed temperature histories in gas tungsten-arc welding of thin plates. Weld J 48(7): 295

22. Goldak J, Chakravarti A, Bibby M (1984) A new finite element model for welding heat sources. Metall Trans B 15(2): 299–305

23. Chen B-Q, Hashemzadeh, Guedes Soares C (2014) Numerical and experimental studies on temperature and distortion patterns in butt-welded plates. Int J Adv Manuf Technol 72: 1121-1131

24. Zhu W-F, Xu C, Zeng L (2010) Coupled finite element analysis of MIG welding assembly on auto-body high-strength steel panel and door hinge. Int J Adv Manuf Technol 51: 551-559

25. Lidam RN, Manurung YHP, Haruman E eta al (2013) Angular distortion analysis of the multipass welding process on combined joint types using thermo-elastic-plastic FEM with experimental validation. Int J Adv Manuf Technol 69: 2373-2386

26. Price J, Paradowska A, Joshi S, Finlayson T (2006) Residual stresses measurements by neutron diffraction and theoretical estimation in a single weld bead. Int J Pres Ves Pip 83: 381-387

27. Deng D, Murakawa H (2008) Prediction of welding distortion and residual stress in a thin plate butt-welded joint. Comput Mater Sci 43: 353-365

28. Pichot F, Danis M, Lacoste E, Danis Y (2013) Numerical definition of an equivalent GTAW heat source. J Mater Process Technol 213(7) 1241-1248

29. Wahab MA, Painter MJ (1997) Numerical models of gas metal arc welds using experimentally determined weld pool shapes as the representation of the welding heat source. Int J Pres Ves Pip 73(2): 153–159

30. Barsoum Z (2007) Residual stress prediction and relaxation in welded tubular joint. Weld World 51(1-2): 23–30

31. Barsoum Z, Barsoum I (2009) Residual stress effects on fatigue life of welded structures using LEFM. Eng Fail Anal 16(1): 449–467

32. Hu J, Tsai HL (2007) Heat and mass transfer in gas metal arc welding. Part I: The arc. Int J Heat Mass Transfer 50(5): 833–846

33. Hu J, Tsai HL (2007) Heat and mass transfer in gas metal arc welding. Part II: The metal. Int J Heat Mass Transfer 50(5): 808–820

34. Xu G, Hu J, Tsai HL (2009) Three-dimensional modeling of arc plasma and metal transfer in gas metal arc welding. Int J Heat Mass Transfer 52(7): 1709–1724

35. Norrish J (1992) Advanced welding processes. Institute of physics

36. Lesnewich A (2003) Commentary on gmaw parameter selection paper

37. Palani PK, Murugan N (2007) Modeling and simulation of wire feed rate for steady current and pulsed current gas meatal arc welding using 317L flux cored wire. Int J Adv Manuf Technol 34:1111-1119

38. Murray PE (2002) Selecting parameters for GMAW using dimensional analysis. Weld J 125-131

39. Modenesi PJ, Reis RI (2007) A model for melting rate phenomena in GMA welding. J Mater Process Technol 189: 199-205

40. Palani PK, Murugan N (2006) Selection parameters of pulsed current gas metal arc welding. J Mater Process Technol 172: 1-10

41. Teng TL, Fung CP, Chang PH (2002) Effect of weld geometry and residual stresses on fatigue in butt-welded joints. Int J Pres Ves Pip 79: 467-482

42. APTA (Asociación para la promoción técnica del acero) document, (On-line). http://apta.com.es/pdf/aceros.pdf. Accessed 11 June 2014

43. GMAW welding guide, Lincoln Electric, (On-line). http://www.oemeyer.com/Media/Default/Industrial/technical/MIG%20welding%20guide-lincoln.pdf. Accessed 11 June 2014

44. Ranjbarnodeh E, Pouranvari M, Fischer A (2013) Influence of welding parameters on residual stresses in dissimilar HSLA steels welds. Association of Metallurgical Engineers of Serbia

45. Pilipenko A (2001) Computer simulation of residual stress and distortion of thick plates in multi-electrode submerged arc welding. Their mitigation techniques. PhD thesis, Norwegian University of Science and Technology

46. Mills KC (2002) Recommended values of thermophysical properties for selected commercial alloys. Woodhead Publishing

47. Thermal conductivity for carbon steel AISI 1010, (On-line). http://www.efunda.com/materials/alloys/carbon_steels/show_carbon.cfm?ID=AISI_1010&show_prop=tc&Page_Title=Carbon%20Steel%20AISI%201010. Accessed 11 June 2014

48. Deng D (2009) FEM prediction of welding residual stress and distortion in carbon steel considering phase transformation effects. Mater Des 30(2): 359–366

49. Pitz M, Merklein M (2005) FE simulation of laser assisted bending. Proceedings of the 11th International Conference: Sheet Metal, pages 745–752

50. Tensile properties at high temperatures for S275 steel, (On-line). http://www.thyssenfrance.com/fich_tech_en.asp?product_id=17930. Accessed 11 June 2014

51. BS EN (2005). Eurocode 3: Design of steel structures-part 1-2: General rules-structural fire design

52. Safety data sheet for Stargon 82, (On-line). http://www.cialgas.com/wp-content/uploads/2012/09/STARGON-82.pdf. Accessed 11 June 2014

53. Larrañaga J (2011) Geometrical accuracy improvement in flexible roll forming process by means of local heating. PhD thesis, Mondragon Unibertsitatea

Figure
Click here to download high resolution image

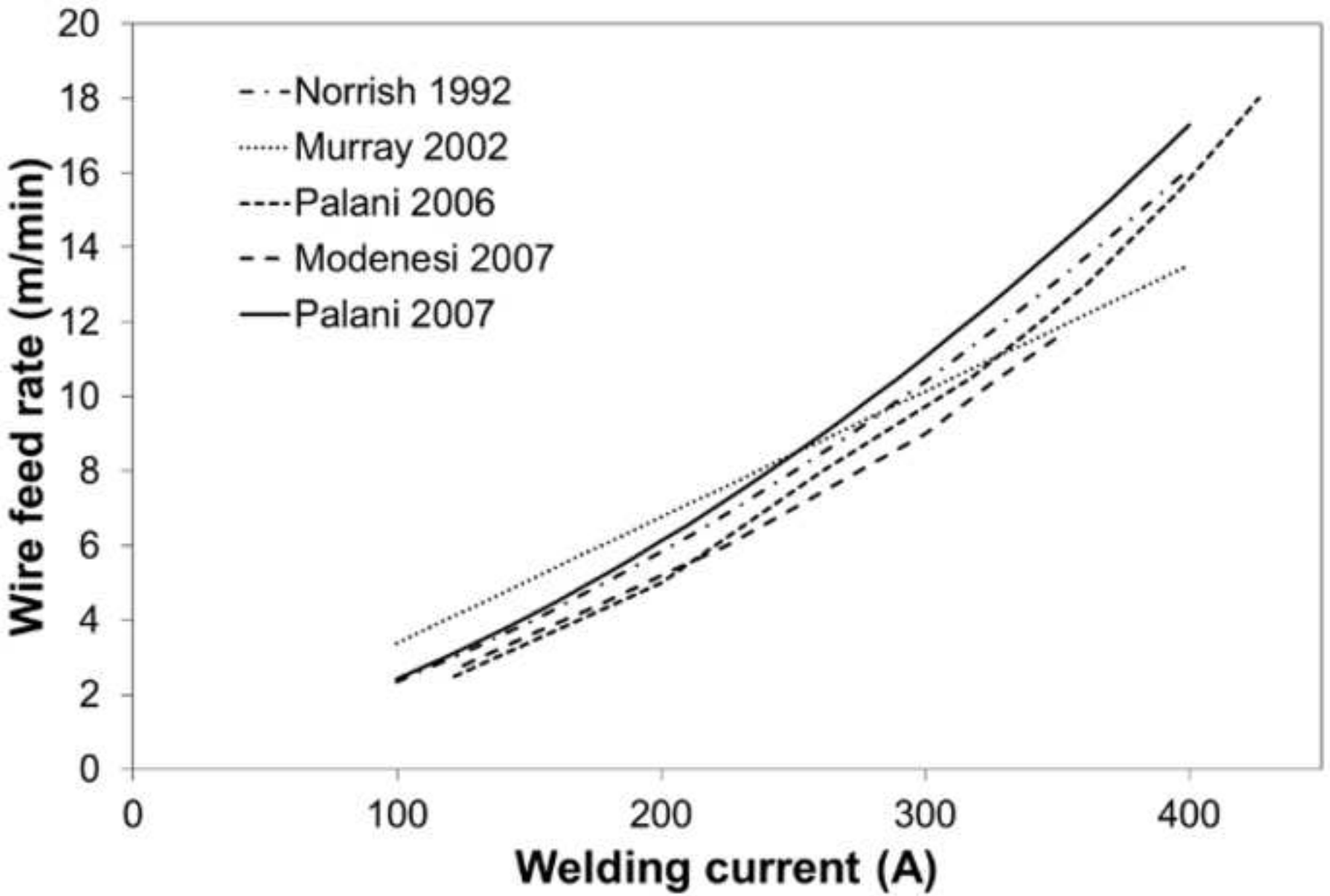

Figure
Click here to download high resolution image

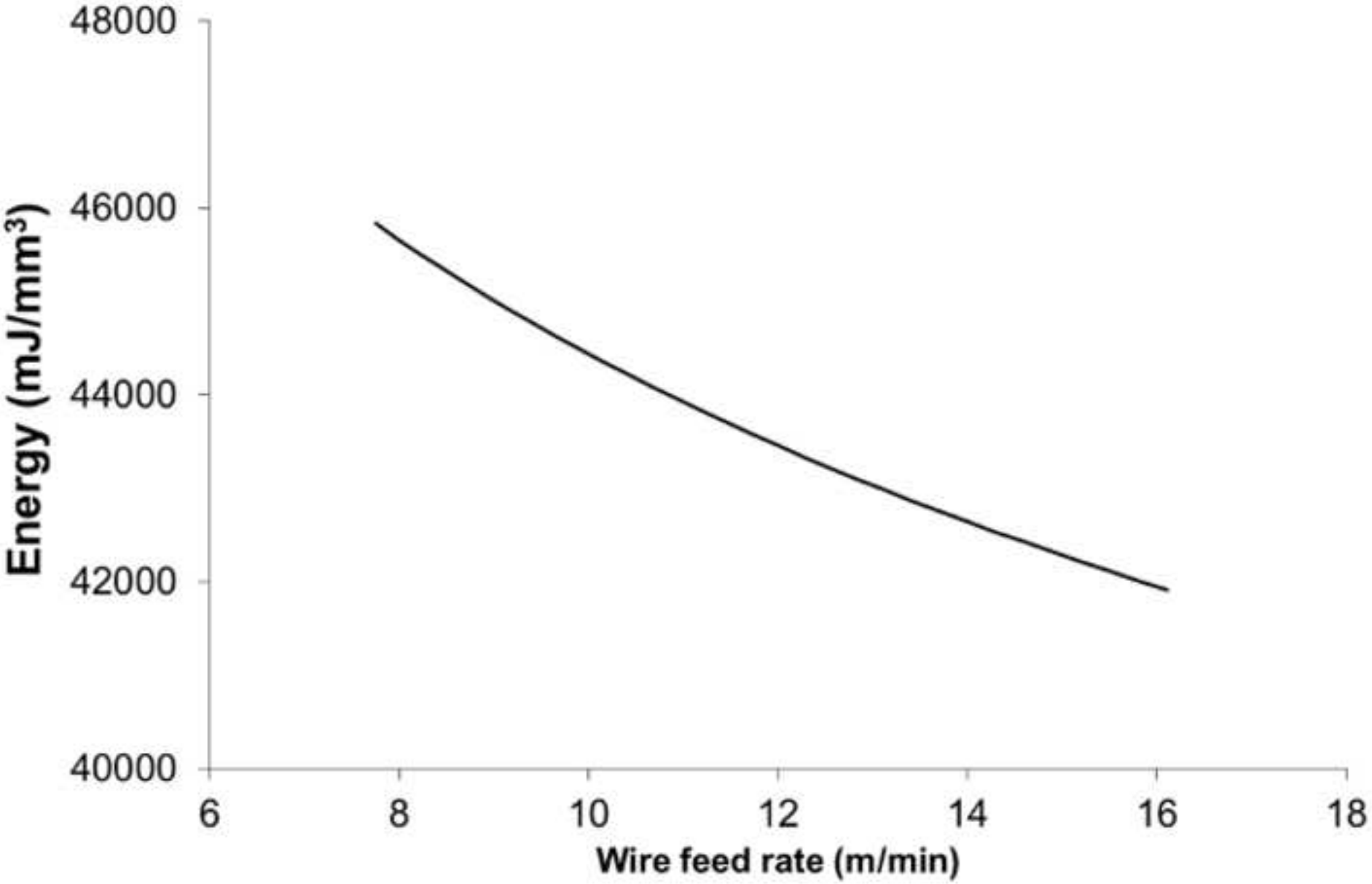

Figure
Click here to download high resolution image

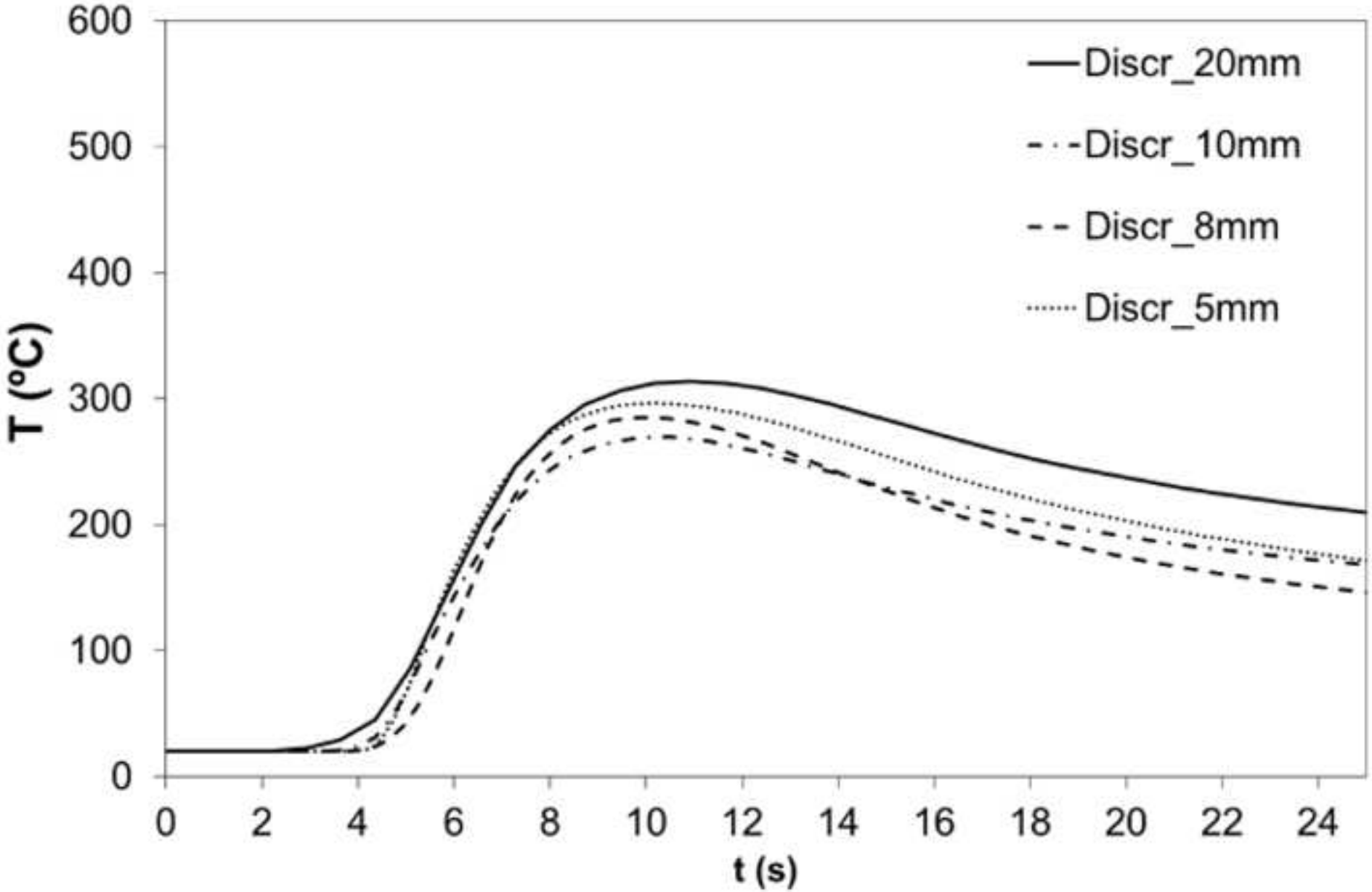

Figure
Click here to download high resolution image

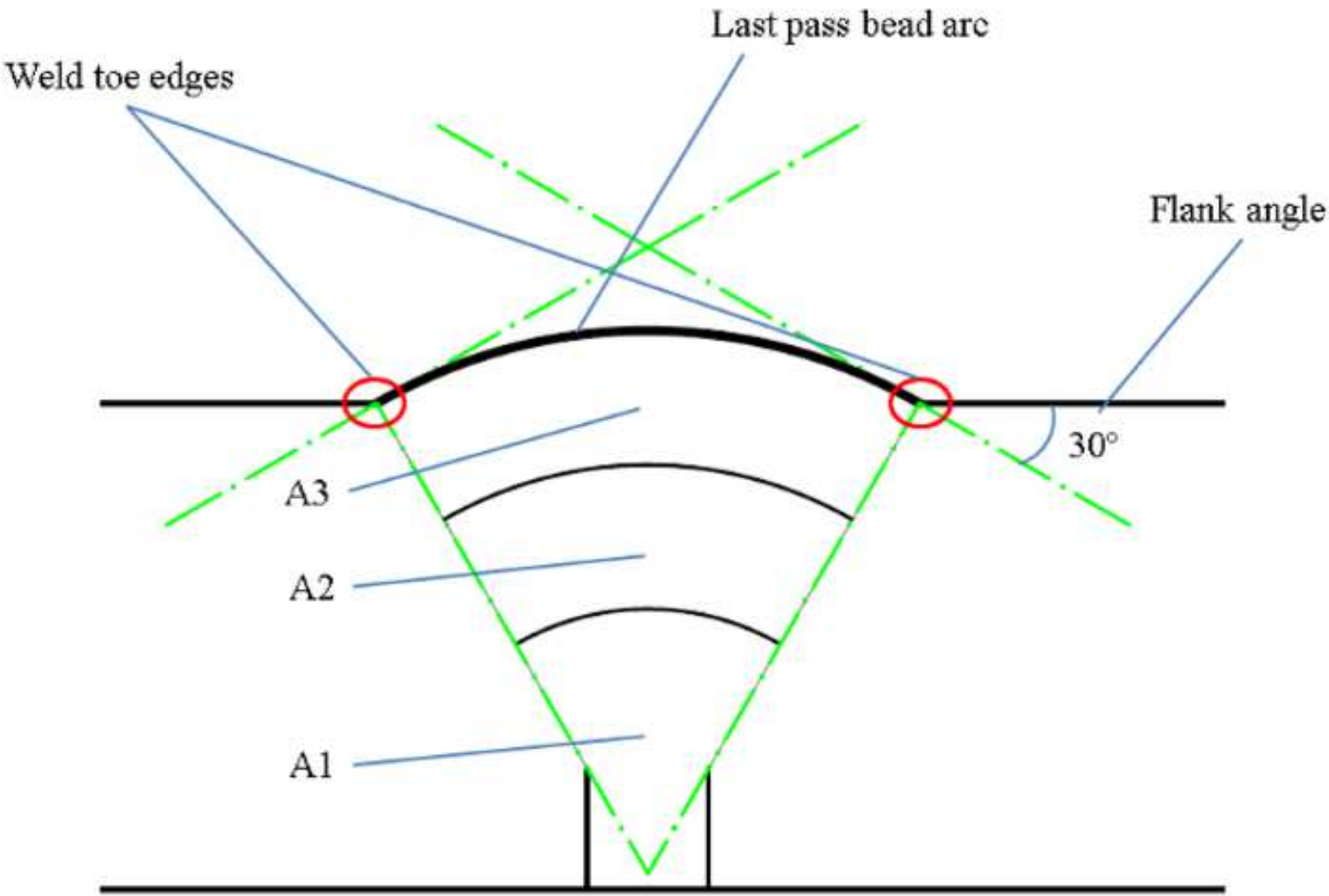

References:

1. Naidu DS, Moore KL, Ozcelik S (2003) Modeling, sensing and control of gas metal arc welding. Kidlington (UK): Elsevier Science Ltd
2. Palani PK, Murugan N (2007) Modeling and simulation of wire feed rate for steady current and pulsed current gas meatal arc welding using 317L flux cored wire. Int J Adv Manuf Technol 34:1111-1119
3. Suban M, Tusek J (2001) Dependence of melting rate in MIG/MAG welding on the type of shielding gas used. J
4. Murray PE (2002) Selecting parameters for GMAW using dimensional analysis. Weld J 125-131
5. Modenesi PJ, Reis RI (2007) A model for melting rate phenomena in GMA welding. J Mater Process Technol 189: 199-205
6. Palani PK, Murugan N (2006) Selection parameters of pulsed current gas metal arc welding. J Mater Process Technol 172: 1-10
7. Norrish J (1992) Advanced welding processes. Institute of physics
8. Deng D (2009) FEM prediction of welding residual stress and distortion in carbon steel considering phase transformation effects. Mater Des 30(2): 359–366
9. Rosenthal D (1941) Mathematical theory of heat distribution during welding and cutting. Weld J 20(5): 220–234
10. Pavelic V, Tanbakuchi R, Uyehara OA, Myers PS (1969) Experimental and computed temperature histories in gas tungsten-arc welding of thin plates. Weld J 48(7): 295
11. Goldak J, Chakravarti A, Bibby M (1984) A new finite element model for welding heat sources. Metall Trans B 15(2): 299–305

12. Barsoum Z, Barsoum I (2009) Residual stress effects on fatigue life of welded structures using LEFM. Eng Fail Anal 16(1): 449–467
13. Hu J, Tsai HL (2007) Heat and mass transfer in gas metal arc welding. Part I: The arc. Int J Heat Mass Transfer 50(5): 833–846
14. Hu J, Tsai HL (2007) Heat and mass transfer in gas metal arc welding. Part II: The metal. Int J Heat Mass Transfer 50(5): 808–820
15. Xu G, Hu J, Tsai HL (2009) Three-dimensional modeling of arc plasma and metal transfer in gas metal arc welding. Int J Heat Mass Transfer 52(7): 1709–1724
16. Teng TL, Fung CP, Chang PH (2002) Effect of weld geometry and residual stresses on fatigue in butt-welded joints. Int J Pres Ves Pip 79: 467-482